

Studies on the Radiation Fraction of Propane Jet Diffusion Flames under Crossflow

Wang J.W.^{1,2}, Fang J.^{1,*}, Zhao L.Y.¹, Lin S.B.¹, Guan J.F.²,
Shah H.R.¹, Zhang Y.M.¹, Sun J.H.¹

¹ University of Science and Technology of China, State Key Laboratory of Fire Science,
Hefei, Anhui, China

² Tsinghua University, Hefei Institute for Public Safety Research, Hefei, Anhui, China

*Corresponding author's email: fangjun@ustc.edu.cn

ABSTRACT

Many industrial combustion devices rely on jet flame combustion in crossflow to achieve mixing and reaction. Studies relating to the determination of the radiation fraction of turbulent jet flames are very important. Previous research affords limited predictive capability regarding the coupling effects of crossflow and jet flow. In this work, a new theoretical prediction equation of radiation fraction is given for its dependence on the fuel mass flow rate and the crossflow velocity. Experiments of turbulent propane jet diffusion flames with 8, 10, 12, and 14 mm exit diameters in 1.0, 1.5 and 2.0 m/s cross-winds were carried out in a wind tunnel. The jet Reynolds numbers varied from 1082 to 4711 and the jet-to-crossflow momentum flux ratio ranged from 0.1 to 10. The experimental results from this work and previous literature show that, the term $\chi_R^{16/11} \dot{m}_j^{4/11} / u_w$ has a good linear relationship with $\dot{m}_j^{1/2} / u_w$, validating the theoretical equation. The radiation fraction is almost independent of the nozzle diameter under low crossflow velocity, and the crossflow has the largest effects on the radiation fraction for smaller nozzle diameters. These occurred mainly because of the effects of crossflow and jet flow velocities on the soot residence time that is proportional to the radiation fraction.

KEYWORDS: Crossflow, propane, radiation fraction, turbulent diffusion flame.

NOMENCLATURE

b_F	flame half width (m)	V_F	flame volume (m ³)
d_j	nozzle exit diameter (m)	Y_s	soot mass fraction (-)
Fr	Froude number (-)	x, y, z	Cartesian coordinates (m)
g	gravitational acceleration (m/s ²)	Greek	
g'	buoyant acceleration (m/s ²)	α	weight coefficient (-)
H	vertical distance between the nozzle and the receptor (m)	ΔH_c	heat of combustion (J/kg)
K_F	parameter (m·s ^{1/2} /kg ^{1/2})	ε	turbulent eddy dissipation rate (m ² /s ³)
K_G	geometric shape parameter (-)	θ	flame tilt angle (degree)
K_S	oxygen-fuel stoichiometric mass ratio (-)	ν	kinematic viscosity (m ² /s)
K_w	stretch factor (s)	ξ	axial ordinate along flame axis (m)
L_F	flame length (m)	ρ	density (kg/m ³)
		σ	Stefan-Boltzmann constant (W/(m ² ·K ⁴))

Proceedings of the Ninth International Seminar on Fire and Explosion Hazards (ISFEH9), pp. 116-124

Edited by Snegirev A., Liu N.A., Tamanini F., Bradley D., Molkov V., and Chaumeix N.

Published by St. Petersburg Polytechnic University Press

ISBN: 978-5-7422-6496-5 DOI: 10.18720/spbpu/2/k19-84

\dot{m}	mass flow rate (kg/s)	τ_k	Kolmogorov time (s)
\dot{m}_{O_2}''	mass flux of oxygen (kg/(s·m ²))	τ_s	soot formation time (s)
\dot{q}''	flame radiation flux at a receiver (W/m ²)	ϕ_s	soot volume fraction (-)
\dot{Q}_R	total radiant power (W)	χ_R	radiation fraction (-)
R	horizontal distance between the nozzle and the receptor (m)	Subscripts	
R_F	distance from flame element to receptor(m)	j	fuel jet
R_M	jet-to-crossflow momentum flux ratios, $R_M = (\rho_j u_j^2) / (\rho_\infty u_w^2)$ (-)	F	flame
T	temperature (K)	s	soot
u	velocity (m/s)	st	stoichiometric condition
		w	crossflow
		0	initial condition of fuel
		∞	ambient

INTRODUCTION

Studies of jet flame in crossflow have been made for a broad range of uses, such as gas turbine combustors, industrial boilers, and flare stacks. In engineering applications, the radiative fraction of a turbulent reacting jet flame in crossflow is very important for the combustion design. Radiation heat emitted from flames is closely related to the thermal stability of the combustors, and is applied widely to design flare systems in the energy and petrochemical industry.

Most of the previous studies have focused on predicting the flame length or trajectory, temperature and radiation fields for the reacting jet in crossflow fields [1-3]. Escudier [4] presented numerical calculations for the variation of bulk temperature and species concentrations along the plume trajectory. Brzustowski [5] modelled the flame as a bent-over, initially vertical and non-buoyant circular jet with top-hat profiles of composition, temperature and velocity. Fairweather et al. [6] predicted the radiative heat flux from field-scale flares, and their study showed that increases in crossflow speed at first decreased soot levels, but eventually led to an increase, once a critical crossflow speed had been exceeded. This effect might be attributed to the crossflow, which at first increases air entrainment rates into the flame, causing a decrease in residence times for soot formation, and then, once the counter rotating vortex pair has been established, increases residence times as the vortex pair grows in strength. Kostiuk et al. [7] conducted research on the flame length of low momentum non-lifted flames (jet-to-crossflow momentum ratio $R_M = (\rho_j u_j^2) / (\rho_\infty u_w^2) < 4.6$), where the velocity of the fuel jet was comparable to that of the crossflow, as typically found in oil-field flares. The data showed two regimes in which the flame length either increased or decreased with increasing wind velocity. Lawal et al. [8] went further to investigate the effect of changes in the fuel exit velocity and the crossflow on the length, radiation fraction, and emission indices of pollutant species (NO_x and CO), as well as the ratio NO₂/NO_x, of a high momentum jet flame in crossflow, with R_M in the range of 100~800.

These previous studies focused more on the separate influences of the crossflow or fuel jet flow on the radiant behaviors of turbulent jet flames. In the present work, the radiation fraction of non-lifted turbulent jet diffusion flames in crossflow was addressed, by considering the coupled effects of the crossflow and jet flow, applicable, but not exclusively, to low R_M ($0.1 < R_M < 10$, $1 < Fr < 100$).

THEORETICAL METHODS

To model the jet diffusion flame, an assumption about its shape is made first. For high-velocity-ratio ($u_j/u_w > 4$, $R_M > 3$ for a variety of fuels) jet diffusion flames, their shape is expected to be approximated by the frustum of a cone (a cone with the tip removed). Experiments showed that the cone half-angle was small at the lowest observed velocity ratio. With increasing crossflow velocity relative to the jet velocity, the flame became nearly cylindrical in shape [1, 9, 10]. In this work, $u_j/u_w < 2.65$ and $0.1 < R_M < 10$, and the assumption of a cylindrical shape without bending would apply. The definitions of the configuration of the tilted flame in crossflow are shown in Fig. 1.

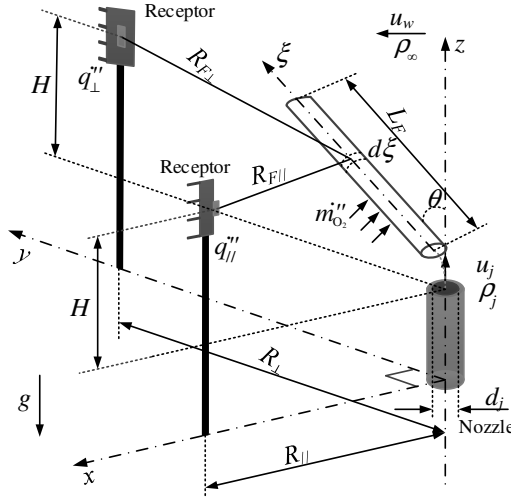


Fig. 1. Configurations of a tilted jet flame in crossflow in Cartesian coordinates. The gas jet discharges at velocity u_j , with density ρ_j from a nozzle of diameter d_j into a crossflow of density ρ_∞ at horizontal velocity u_w ; ξ is the axial ordinate in y - z plane; $d\xi$ is the flame element.

The flame radiation fraction χ_R , is defined as the ratio of the total radiant power \dot{Q}_R emitted from the flame to the total heat release rate, which is given as:

$$\chi_R = \frac{\dot{Q}_R}{\dot{m}_j \Delta H_c} = \frac{\sigma T_F^4 A_F [1 - \exp(-\kappa L)]}{\dot{m}_j \Delta H_c} \sim \frac{\sigma T_F^4 V_F \phi_s}{\dot{m}_j \Delta H_c}, \quad (1)$$

where \dot{m}_j is the fuel jet mass flow rate (mg/s), ΔH_c the heat of combustion (J/kg), σ Stefan-Boltzmann constant, 5.67×10^{-8} W/(m²·K⁴), T_F the flame temperature (K), A_F the flame surface area (m²), κ the soot absorption coefficient (1/m), L the flame mean optical length (m), V_F the flame volume (m³), and ϕ_s the soot volume fraction. For an optical thin flame, the flame emissivity, $1 - \exp(-\kappa L)$, can be simplified to κL ; in addition, $\kappa \sim \phi_s$. Therefore, as shown in Eq. (1), the flame radiation fraction is an overall characteristic of the flame, which can be affected by flame temperature, soot formation, flame type, combustion efficiency, ambient conditions, etc.

For a cylinder flame model, the flame volume V_F is related to the flame diameter and length. The flame diameter (or half-width b_F) changes in proportion to the flame length, based on the assumption that the jet flame retains self-similarity in crossflow as [11]:

$$2\bar{b}_F = K_G L_F, \quad (2)$$

where the geometric shape parameter, $K_G = 0.23(\rho_{st}/\rho_j)^{1/2}$. Hence, the flame volume can be represented by the mean flame length, as:

$$V_F = \frac{\pi}{4}(2\bar{b}_F)^2 L_F = \frac{\pi}{4} K_G^2 L_F^3. \quad (3)$$

The soot volume fraction ϕ_s or the soot mass fraction Y_s inside the turbulent flame envelope depends on the ratio of the characteristic flow time to soot formation time, τ_s . Generally, the magnitude of the characteristic flow time is determined by the local straining action of the turbulent flow field [12]. Therefore,

$$\phi_s \frac{\rho_s}{\rho} \sim Y_s \sim \frac{\tau_k}{\tau_s}, \quad (4)$$

where the Kolmogorov time scale is $\tau_k = \sqrt{\nu/\varepsilon}$, the turbulent eddy dissipate rate $\varepsilon \sim u_F^3/L_F$ and ν is the kinematic viscosity (m^2/s). Here, u_F and L_F are identified to be the characteristic buoyant flow velocity and flame length for the flame region, so $u_F \sim \sqrt{2g'L_F}$, where buoyant acceleration $g' = (\Delta\rho/\rho)g$.

The soot formation time τ_s is basically dependent on the fuel chemistry and the thermochemical parameters of the combustion system, thus Eq. (4) can be recast as:

$$Y_s \sim \frac{\nu^{1/2} g'^{-3/4}}{\tau_s} L_F^{-1/4}. \quad (5)$$

Additionally, the flame radiation has a negative feedback to the flame temperature, from the dependence of radiation fraction on the laminar smoke point height, as [13]:

$$\sigma T_F^4 \sim \chi_R^{-3}. \quad (6)$$

So, combining Eqs. (3), (5) and (6), Eq. (1) can be re-written as:

$$\chi_R^4 \sim \frac{\pi K_G^2 L_F^{11/4}}{4 \dot{m}_j \Delta H_c} \sim \frac{L_F^{11/4}}{\dot{m}_j \Delta H_c}. \quad (7)$$

For a low momentum jet diffusion flame length in crossflow, Majeski *et al.* [9] assumed that the mean oxygen mass flux to the flame surface (\dot{m}_{O_2}'') was constant, and the size of the flame was set by the time required for the diffusion of the stoichiometric amount of oxygen and fuel jet. Furthermore, in crossflow the stretching length was expected to be directly proportional to the crossflow velocity with constant timescale proportionality. So the mean jet flame length is proposed to be:

$$L_F = K_F (\rho_j u_j)^{1/2} d_j + K_w u_w. \quad (8)$$

Since $(\rho_j u_j)^{1/2} d_j = \sqrt{4\dot{m}_j/\pi}$, Eq. (8) can be recast as:

$$L_F \sim K_F (\dot{m}_j)^{1/2} + K_w u_w, \quad (9)$$

where $K_F^2 = K_S / (\pi K_G \dot{m}_{O_2}^{\prime\prime})$, $K_w = \partial L_F / \partial u_w$ is a stretch factor of the flame length with regard to crossflow velocity, and K_S is the oxygen-fuel stoichiometric mass ratio.

Substituting Eq. (9) into Eq. (7), yields

$$\chi_R^4 \sim \frac{1}{\dot{m}_j} (K_F \dot{m}_j^{1/2} + K_w u_w)^{11/4}. \quad (10)$$

Equation (10) can be re-arranged into the following final form:

$$\frac{\chi_R^{16/11} \dot{m}_j^{4/11}}{u_w} \sim K_F \frac{\dot{m}_j^{1/2}}{u_w} + K_w. \quad (11)$$

EXPERIMENTAL SETUP

A diagram of the experimental setup is shown in Fig. 2. All experiments were carried out in a wind tunnel facility located in SKLFS of USTC. Its test section is 6 m long, 1.8 m wide and 1.8 m high, which has a stable longitudinal airflow to simulate crossflow between 0.5 and 15 m/s with turbulence fluctuation intensity less than 2%. Four hot-wire anemometers, with an accuracy of 0.01 m/s, were used to measure the transient velocity of the crossflow.

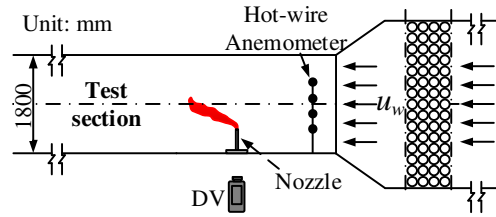


Fig. 2. Diagram of the experiment.

The circular nozzle was in the middle of the test section, and its exit plane was 50 cm above the bottom of the tunnel to reduce the influence of the boundary layer of the tunnel. Propane was used as the fuel and the flow supplied to the vertical jet was measured and controlled by an Alicat mass flow meter with a precision of $\pm(0.8\%$ of reading + 0.2% of full scale). The fuel mass flow rate was in the range of 105–241 mg/s, and the diameters of the nozzles were 8, 10, 12, and 14 mm. The Reynold number and Froude number of the fuel jet were 2016–4711 and 1–100, respectively. The momentum flux ratio R_M was 0.1–10. More details appear in [10].

A color CCD camera, capturing 25 frames per second, recorded video images of the flame from a glass observation window outside of the wind tunnel. Two radiant heat flux sensors (TS-30, Captec Co. Ltd) with a resolution of 1.5 W/m^2 , facing and parallel to the flame, as shown in Fig. 1, measured the flame radiation flux.

The use of ground-based measured radiant flux to obtain the radiation fraction of a turbulent jet diffusion flame presents a challenging task. Two integral models, IPS (Integrated Punctual Source) and IDS (Integrated Diffuse Source), lead to the expressions in Eq. (12), as shown in:

$$\chi_R = \begin{cases} 4\pi L_F \dot{q}'' \left(\dot{m}_j \Delta H_c \int_0^{L_F} 1/R_F^2 d\xi \right)^{-1}, & \text{IPS model} \\ \pi^2 L_F \dot{q}'' \left(\dot{m}_j \Delta H_c \int_0^{L_F} \cos \theta / R_F^2 d\xi \right)^{-1}, & \text{IDS model} \end{cases} \quad (12)$$

The IPS model expects a long thin flame to be comprised of a series of point sources each radiating uniformly over 4π steradians, with the assumption that the flame itself is completely transparent to radiation and the one-point sources will not interfere with each other. The IDS model assumes that the flame is completely opaque so that the radiation emanates from the surface of the flame envelope. Application of these models to data shows that the IPS model over-predicts in the near field, while the IDS under-predicts near the jet flame.

To counteract the over and under prediction weakness of the two models, McMurray [14] combined them to provide a mixing model (Integrated Mixing Source) as follows:

$$\chi_R (\text{IMS}) = \alpha \chi_R (\text{IPS}) + (1 - \alpha) \chi_R (\text{IDS}), \quad (13)$$

Where α is the weight coefficient.

Here the IMS model was applied to the two receptors expressed as Eq. (13) with $\alpha = 0.5$. The time-averaged radiant flux, flame length and tilt angle were substituted into Eq. (14), allowing for the calculation of $\bar{\chi}_R$ by numerical solution of the integrals:

$$\bar{\chi}_R = 0.5(\chi_{R_\perp} + \chi_{R_{//}}), \quad (14)$$

where

$$\chi_{R_\perp} = \frac{2\pi L_F \dot{q}''_\perp}{\dot{m}_j \Delta H_c \cdot \int_0^{L_F} 1/R_{F_\perp}^2 d\xi} \left(1 + \frac{\pi}{4 \cos \theta} \right), \quad \chi_{R_{//}} = \frac{2\pi L_F \dot{q}''_{//}}{\dot{m}_j \Delta H_c \cdot \int_0^{L_F} 1/R_{F_{//}}^2 d\xi} \left(1 + \frac{\pi}{4 \cos \theta} \right),$$

$$R_{F_\perp}^2 = (H_R - \xi \cdot \cos \theta)^2 + (R_\perp - \xi \cdot \sin \theta)^2, \quad R_{F_{//}}^2 = (H_R - \xi \cdot \cos \theta)^2 + (R_{//} - \xi^2 \cdot \sin^2 \theta).$$

RESULTS AND DISCUSSION

Imaging analysis

For the flickering flame, by image processing, its slant length was determined by measuring the distance between the center of the nozzle exit and the “peak” of the contour of fifty percent of flame occurrence probability as Fig. 3 shows [15]. The flame tilt angle was also obtained by the vector of the mean flame length.

Sequential images of the visible flame for different momentum ratio values are shown in Fig. 4. It can be seen that the continuous regions of the flames in crossflow were more stable and longer than the purely buoyant flames, where the shear effect of the transverse stream caused concentration of vorticity, evolving to form vortex structures transported downstream. Buoyancy had more effects downstream, where there were flickering movements in the tip. The flame was bent near the nozzle, with a cylindrical shape and a steady tilt angle. With increase in R_M , the flame tilt angle decreased.

χ_R dependence on \dot{m}_j and u_w

Figure 5 plots the variations of radiation fraction with fuel mass flow rate under different crossflow velocities. In Fig. 5(a), the radiation fraction was almost independent of the nozzle diameter under low crossflow velocity, while in Fig. 5(b) and (c) it increased with the nozzle diameter, because the

increasing crossflow velocity stretches the flame and increases the velocity of the hot gas leading to lower soot residence time τ_{res} ($\sim \tau_k \sim \phi_s \sim \chi_R$) [16].

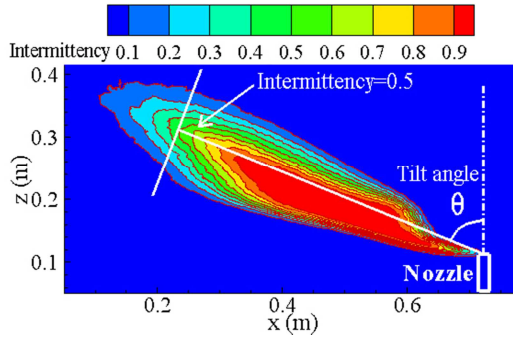


Fig. 3. Determination of flame tile angle from flame images ($d_j = 10$ mm, $u_j = 1.49$ m/s, $u_w = 2.0$ m/s).

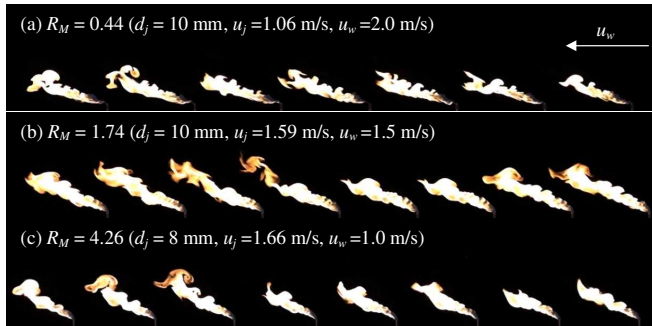


Fig. 4. Sequential visible flame images with different R_M values.

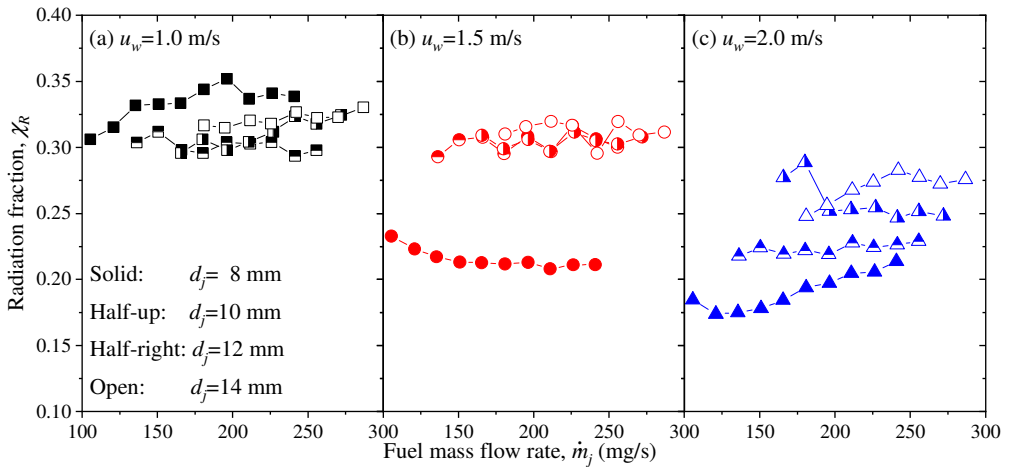


Fig. 5. Variations of radiation fraction with the fuel mass flow rate and crossflow velocity.

Additionally, for the cases of $d_j = 8$ mm, the crossflow has the biggest effects on the radiation fraction, as compared with other cases. This occurred because the flame jet had the largest velocity

variation, accompanied with the great change of soot residence time τ_{res} that is proportional to the radiation fraction. For the cases of $d_j = 10\text{-}14$ mm, due to the relative larger jet velocity, the effects of crossflow on the radiation fraction were small, so the radiation fraction almost remained unchanged for jet diameters of $d_j = 10$ and 12 mm, and decreased slightly.

The flame radiation fraction, when correlated with the fuel flow rate and crossflow velocity based on Eq. (11) as shown in Fig. 6, exhibits good linearity. The data of Brzustowski et al. [17] are also shown for comparison.

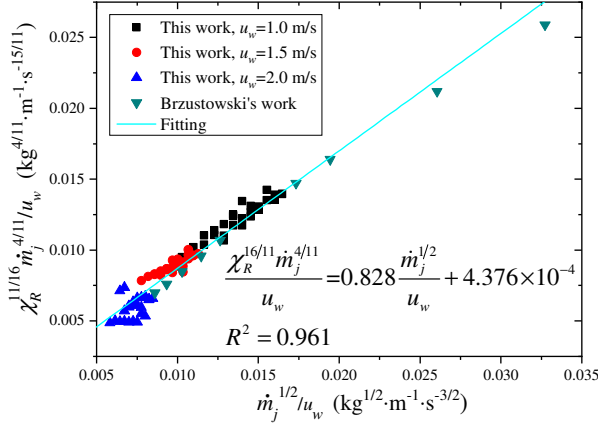


Fig. 6. Flame radiation fraction correlating to the fuel mass flow and crossflow velocity based on Eq. (11).

As the physical and thermochemical parameters including τ_s , v and ΔH_c are independent of \dot{m}_j and u_w , from Eq. (11), the full derivative of χ_R remains proportional to du_w and $d\dot{m}_j$:

$$d\chi_R \sim \frac{11}{16} K_w \dot{m}_j^{-4/11} \chi_R^{-5/11} du_w + \frac{1}{16} \chi_R^{-5/11} \left(\frac{3}{2} K_F \dot{m}_j^{-19/22} - 4 K_w u_w \dot{m}_j^{-15/11} \right) d\dot{m}_j. \quad (15)$$

It was found that, when the flame shape parameter $\psi_F = \sqrt{4/\pi} \dot{m}_j^{1/2} / u_w > 6.74 \times 10^{-3}$ ($\text{kg} \cdot \text{s} / \text{m}^2$)^{1/2}, $K_w > 0$ [9], wind will stretch the flame instead of shrinking. This occurs in most cases considered in this work ($0.0175 > \psi_F > 0.0058$).

CONCLUSIONS

The radiation fraction for non-lifted turbulent jet flames with low-momentum ratios has been addressed by considering the coupling effects of the crossflow and jet flow. The main conclusions are:

- (1) A new theoretical prediction equation of radiation fraction has been developed, incorporating the fuel mass flow rate and crossflow velocity. The parameter $\chi_R^{16/11} \dot{m}_j^{4/11} / u_w$ displays a good linear relationship with $\dot{m}_j^{1/2} / u_w$.
- (2) The radiation fraction is almost independent of the nozzle diameter under low crossflow velocity and the crossflow has the biggest effect on the radiation fraction for the smaller nozzle diameter. These trends are mainly due to the impact of crossflow and jet flow velocities on the soot residence time that is proportional to the radiation fraction.

ACKNOWLEDGEMENTS

This work was supported by the National Natural Science Foundation of China (grant numbers: 51576186, 51636008); National Key R&D Program (2016YFC0801500); NSFC-STINT joint project (USTC-Lund University). Key Research Program of the Chinese Academy of Sciences (QYZDB-SSW-JSC029); Fundamental Research Funds for the Central Universities (WK2320000034, WK2320000036); China Postdoctoral Science Foundation funded project (2018M632549); and the Open Project Program of State Key Laboratory of Fire Science (HZ2018-KF03).

REFERENCES

- [1] J. Wang, J. Fang, J. Guan, Y. Zhang, J. Sun, Effect of crossflow on the air entrainment of propane jet diffusion flames and a modified Froude number, *Fuel* 233 (2018) 454-460.
- [2] Q. Wang, L.H. Hu, X. Zhang, X. Zhang, S. Lu, H. Ding, Turbulent jet diffusion flame length evolution with cross flows in a sub-pressure atmosphere, *Energy Convers. Manag.* 106 (2015) 703-708.
- [3] X. Zhang, W. Xu, L. Hu, X. Liu, X. Zhang, W. Xu, A new mathematical method for quantifying trajectory of buoyant line-source gaseous fuel jet diffusion flames in cross air flows, *Fuel* 177 (2016) 107-112.
- [4] M.P. Escudier, Aerodynamics of a burning turbulent gas jet in a crossflow, *Combust. Sci. Technol.* 4 (1971) 293-301.
- [5] T.A. Brzustowski, The hydrocarbon turbulent diffusion flame in subsonic cross-flow, In: *The hydrocarbon turbulent diffusion flame in subsonic cross-flow*, Los Angeles, California, 1977, pp. 24-26.
- [6] M. Fairweather, W.P. Jones, R.P. Lindstedt, Predictions of radiative transfer from a turbulent reacting jet in a cross-wind, *Combust. Flame* 89 (1992) 45-63.
- [7] L.W. Kostiuik, A.J. Mejeski, P. Poudenx, M.R. Johnson, D.J. Wilson, Scaling of wake-stabilized jet diffusion flames in a transverse air stream, *Proc. Combust. Inst.* 28 (2000) 553-559.
- [8] M.S. Lawal, M. Fairweather, D.B. Ingham, L. Ma, M. Pourkashanian, A. Williams, Numerical Study of Emission Characteristics of a Jet Flame in Cross-Flow, *Combust. Sci. Technol.* 182 (2010) 1491-1510.
- [9] A.J. Majeski, D.J. Wilson, L.W. Kostiuik, Predicting the Length of Low-Momentum Jet Diffusion Flames in Crossflow, *Combust. Sci. Technol.* 176 (2004) 2001-2025.
- [10] J.W. Wang, J. Fang, S.B. Lin, J.F. Guan, Y.M. Zhang, J.J. Wang, Tilt angle of turbulent jet diffusion flame in crossflow and a global correlation with momentum flux ratio, *Proc. Combust. Inst.* 36 (2017) 2979-2986.
- [11] N. Peters, *Turbulent Combustion*, Cambridge University Press, Cambridge, U.K., 2004.
- [12] L.H. Hu, Q. Wang, M.A. Delichatsios, S.X. Lu, F. Tang, Flame radiation fraction behaviors of sooty buoyant turbulent jet diffusion flames in reduced- and normal atmospheric pressures and a global correlation with Reynolds number, *Fuel* 116 (2014) 781-786.
- [13] J.W. Wang, J. Fang, J.F. Guan, Y. Zeng, Y.M. Zhang, Flame volume and radiant fraction of jet diffusion methane flame at sub-atmospheric pressures, *Fuel* 167 (2016) 82-88.
- [14] R. McMurray, Flare radiation estimated, *Hydrocarb. Process.* 61 (1982) 175-181.
- [15] M.J. Hurley, D.T. Gottuk, J.R. Hall Jr, K. Harada, E.D. Kuligowski, M. Puchovsky, J.M. Watts Jr, C.J. Wiecek, *SFPE Handbook of Fire Protection Engineering*, 5th ed., Springer, 2015.
- [16] M.A. Delichatsios, L. Orloff, Effects of turbulence on flame radiation from diffusion flames, *Proc. Combust. Inst.* 22 (1989) 1271-1279.
- [17] T.A. Brzustowski, S. Gollahalli, M. Gupta, M. Kaptein, H. Sullivan, Radiant heating from flares, ASME paper 75-HT-4 (1975).